# Photoelectron Circular Dichroism in the Spin-Polarized Spectra of Chiral Molecules

A. N. Artemyev,[1] R. Tomar,[2] D. Trabert,[2] D. Kargin,[3] E. Kutscher,[1] M. S. Schöffler,[2] L. Ph. H. Schmidt,[2] R. Pietschnig,[3] T. Jahnke,[4,5] M. Kunitski,[2] S. Eckart,[2] R. Dörner,[2,*] and Ph. V. Demekhin[1,†]

[1]*Institut für Physik und CINSaT, Universität Kassel, Heinrich-Plett-Straße 40, 34132 Kassel, Germany*
[2]*Institut für Kernphysik, Goethe-Universität, Max-von-Laue-Straße 1, 60438 Frankfurt am Main, Germany*
[3]*Institut für Chemie und CINSaT, Universität Kassel, Heinrich-Plett-Straße 40, 34132 Kassel, Germany*
[4]*Max-Planck-Institut für Kernphysik, Saupfercheckweg 1, 69117 Heidelberg, Germany*
[5]*European XFEL, Holzkoppel 4, 22869 Schenefeld, Germany*

(Received 22 December 2023; revised 26 January 2024; accepted 26 February 2024; published 22 March 2024)

We studied strong-field multiphoton ionization of 1-iodo-2-methylbutane enantiomers with 395 nm circularly polarized laser pulses experimentally and theoretically. For randomly oriented molecules, we observe spin polarization up to about 15%, which is independent of the molecular enantiomer. Our experimental findings are explained theoretically as an intricate interplay between three contributions from HOMO, HOMO-1, and HOMO-2, which are formed of 5p-electrons of the iodine atom. For uniaxially oriented molecules, our theory demonstrates even larger spin polarization. Moreover, we predict a sizable enantiosensitive photoelectron circular dichroism of about 10%, which is different for different spin states of photoelectrons.

DOI: 10.1103/PhysRevLett.132.123202

Interaction of circularly polarized light with matter gives rise to many dichroic phenomena. One such effect, present for chiral molecules, is known as photoelectron circular dichroism (PECD, [1–3]). The PECD is a helicity and enantiospecific forward-backward asymmetry in the photoelectron emission (with respect to the light propagation direction) occurring independent of the spatial orientation of the molecule, i.e., for randomly oriented molecules. It arises in the electric-dipole light-matter interaction. In particular, in the presence of a chiral potential, circularly polarized light couples differently to different projections $m_\ell$ (magnetic quantum numbers) of the photoelectron angular momentum $\ell$. Being predicted theoretically almost half a century ago [4], PECD was observed much later, first, in the one-photon ionization of chiral molecules [5,6] and then in the multiphoton ionization [7,8], as well. Because of this universality with respect to the photoionization regime [9,10], this chiroptical effect became nowadays a powerful tool for determination of enantiomeric excess of molecular samples in the gas phase with sub-percent sensitivity [11].

Another dichroic effect, also present within the electric-dipole approximation, which was predicted also first theoretically [12] more than half a century ago, is the spin polarization of photoelectrons ionized by circularly polarized light. It emerges due to the spin-orbit (SO) interaction and relies on the fact that different projections $m_\ell$, which couple to circularly polarized light, combine statistically in different ways with the spin projections $m_s = \pm\frac{1}{2}$ to produce photoelectron states with particular total angular momentum $j$ and its projection $m_j$. Most of the earlier experimental and theoretical studies of this effect considered one-photon ionization of atoms and molecules [13,14]. Motivated by the recent theoretical prediction of a huge spin polarization in strong-field tunnel ionization of noble gas atoms [15], several experimental [16,17] and theoretical [18–23] studies on spin polarization in strong-field ionization of atoms and molecules were reported in the last ten years. Those works observed up to 60% spin polarization [17] and formulated propensity rules for the effect in the strong-field multiphoton and tunnel ionization limits [21].

Starting about 25 years ago (and studied more actively in the last decade) [24–26], it was shown that chiral molecules can be used as efficient spin filters for electrons emitted from a surface. In particular, a spin polarization of up to 60% has been found in [24] for photoelectrons traversing a self-assembled monolayer of chiral molecules adsorbed on a surface, and the most recent record for small molecules is almost 90% [27]. It is assumed that such an effect might be related to the exponential sensitivity of the tunneling probability for traveling electrons, which is modified by the SO interaction and the chiral asymmetry of the potential. In the present Letter, we show that a directionally asymmetric abundance of spin-polarized electrons can occur not only as a transport phenomenon but has its

origin in the photoelectron emission process itself when considering chiral molecules. We propose a corresponding mechanism, that combines the two dichroic effects discussed above. In particular, we observe a 15% spin polarization for the strong-field multiphoton ionization of randomly oriented chiral 1-iodo-2-methylbutane (IMB) molecules. In addition, our theory predicts much stronger spin polarization even if only one molecular axis is fixed in space (as, e.g., on a surface). Importantly, we theoretically demonstrate that the forward-backward asymmetry of photoelectrons caused by the molecular chirality (the PECD) substantially depends on the photoelectron's spin polarization.

The present experiment was performed similarly to that of our previous work on spin polarization in multiphoton ionization of Xe [17] with 395 nm pulses, for which above-threshold ionization (ATI) peaks can be identified and a larger effect (as compared to 780 nm pulses [16]) is observed. Laser pulses of 790 nm with a duration of 40 fs generated by a KMLabs Wyvern 500 Ti:sapphire chirped pulse amplification laser system were frequency-doubled to produce 395 nm pulses using a $\beta$-barium borate crystal. Thereafter, a quarter-wave plate and a lens with a focal distance of 200 mm were used to create circularly polarized pulses with the focal-average peak intensity of $3 \times 10^{13}$ W/cm$^2$. The measurements were performed with two enantiopure 1-iodo-2-methylbutane samples, covering prepared synthetically $R(-)$ enantiomer and commercially available $S(+)$ enantiomer (Sigma Aldrich). The photoelectrons were guided through a time-of-flight spectrometer to a commercial Mott spin polarimeter [28]. The acceptance solid angle was enhanced using two different electrostatic lenses, as described in Ref. [17]. A possible asymmetry in detector efficiencies was excluded by inverting the light helicity every 5 min, with the total acquisition time of 14 h for each enantiomer. The measured time-of-flight spectra are converted into (spin-polarization-dependent) kinetic energy spectra using the known [29] instrumental scaling factor of the Mott detector as described in Ref. [17].

Our experimental results are depicted in Fig. 1. Its panel (a) shows the electron-energy spectra of both IMB enantiomers. The spectra exhibit continuous electron distributions, which decline by 3 orders of magnitude within a range from 0 to about 7 eV kinetic energy. Three humps can be identified in the spectra at kinetic energies below 1 eV, in between 2 and 4 eV, and from 5 to 7 eV. The energy spacing of around 3 eV in between the humps fits well to the photon energy of 3.14 eV (which corresponds to the wavelength of 395 nm). As will become evident below, the threshold peak is produced by three-photon ionization, and the high-energy peaks via four- and five-photon ATI, respectively. The experimental spectrum is the product of the real spectrum and an energy dependent response function of the spectrometer and the Mott detector. This response function is not exactly known but it decreases steeply with electron energy. We note that this response function is spin

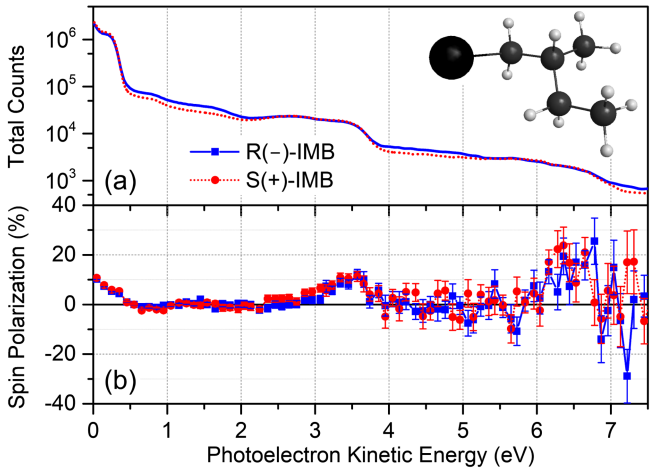


FIG. 1. Results of our experiment performed for randomly oriented $R(-)$ and $S(+)$ enantiomers of IMB with 395 nm circularly polarized laser pulses of $3 \times 10^{13}$ W/cm$^2$ peak intensity and positive helicity. Panel (a): the total photoelectron spectra for both enantiomers. The spectra are distorted by the instrumental response function; see text for details. The $R(-)$-IMB enantiomer is shown in the inset. Panel (b): spin polarization for both enantiomers. The error bars represent statistical uncertainties.

independent as it is caused by the electrostatic lens in the time-of-flight spectrometer. Figure 1(b) depicts the measured spin polarization as a function of the electron kinetic energy. For brevity, photoelectrons with the projections $s_z = +\frac{1}{2}$ and $s_z = -\frac{1}{2}$ of their spin $\vec{s}$ on the propagation direction of circularly polarized light are designated below as spin-↑ and spin-↓. The depicted spin polarization is obtained as the normalized difference between the respective spectra $\{[(\uparrow) - (\downarrow)]/[(\uparrow) + (\downarrow)]\}$ [15–18]. As one can see, at photoelectron energies corresponding to the photon ionization and two ATI peaks in the spectrum, we observe a large spin polarization of up to +15%. Interestingly, the measured spin polarization is almost independent of the enantiomer.

In order to understand our experimental findings, we performed quantum mechanical calculations of the considered photoionization process using the time-dependent single center method [30], which was previously applied to study angle-resolved photoionization spectra of chiral molecules [31–35]. In particular, we employed its latest modification [23], which allowed us to explain the recent experiments on spin polarization in multiphoton ionization of Xe atom [17]. The method consists of a simultaneous propagation of spin-↑ and spin-↓ single-active-electron wave packets in terms of spherical spinors, driven by the laser pulses in the ionic potential, which explicitly includes the SO interaction. Below, we summarize computational details relevant for the present study of the IMB molecule. In order to create a proper chiral ionic potential for active photoelectrons, we first generated Hartree-Fock electronic orbitals of the molecule at its neutral equilibrium geometry.

The nuclei and bound electrons were included in the electrostatic potential. The hole in the molecular ion was symmetrically distributed over three outer orbitals (i.e., HOMO, HOMO-1, and HOMO-2), which are mainly build of the 5p-electrons of the iodine atom. This choice is justified by a theoretical study on the HI molecule (which we additionally performed), where experimental ionization potentials of the relevant HOMO-$n$ are known. The single center expansion of the photoelectron wave packet was restricted by partial harmonics with $\ell, |m| \leq 20$.

The ionic potential included only the spherical part of the SO interaction [see Eq. (3) in Ref. [23] ], as generated by the iodine atom (with the heaviest nuclear charge $Z = 53$). To be able to use this equation, the center of the molecule was placed at the location of the iodine atom. The main contribution to the SO interaction, which diverges as $\sim(Z/r^3)$, comes from the spatial region very close to the iodine nucleus. To properly describe this interaction, the employed radial box of 150 a.u. was divided into 52 finite elements of different size, with more elements very close to the origin. These finite elements were covered by normalized Lagrange interpolating polynomials constructed over Gauss-Lobatto points [36,37]. In addition, the ionic potential included a local electrostatic exchange interaction, as given in the $X\alpha$ approximation [38]. We optimized the radial grid and $X\alpha$ parameter such that employing this procedure to Xe atom yields proper binding energies and, thus, the SO splitting of its $5p_{1/2}$- and $5p_{3/2}$-electrons. Thereby, diagonalization of the one-electron stationary Hamiltonian for the IMB molecule, yielded the binding energies: 8.95 eV for the doubly degenerate states no. 94 and no. 93 (HOMO), 9.67 eV for the states no. 92 and no. 91 (HOMO-1), and 11.00 eV for no. 90 and no. 89 (HOMO-2), as enumerated from the lowermost one (note that the IMB molecule has 94 electrons).

As in our previous theoretical work on Xe [23], the photoelectron wave packets for the orbitals nos. 89–94 of the IMB molecule were propagated in terms of all eigenstates of the stationary Hamiltonian with energies up to +1.0 a.u. For this purpose, we employed the FEAST solver package [39,40], which provides accurate eigenstates within a given interval of eigenvalues (see also Ref. [41] for details on this strategy). We used a sine-squared 395 nm circularly polarized laser pulses with a peak intensity of $10^{13}$ W/cm$^2$, which supports six optical cycles (corresponding to the total propagation time of about 8 fs). To obtain the photoelectron spectra after the pulse was over, the wave packets for spin-↑ and spin-↓ photoelectrons, constructed over the eigenstates with positive energies, were separately projected on the Coulomb functions. To simulate freely rotating molecules in the gas phase, the calculations were performed for (and subsequently averaged over) different orientations of the molecule in the laboratory frame in steps of $0.2\pi$ of two relevant orientation Euler angles.

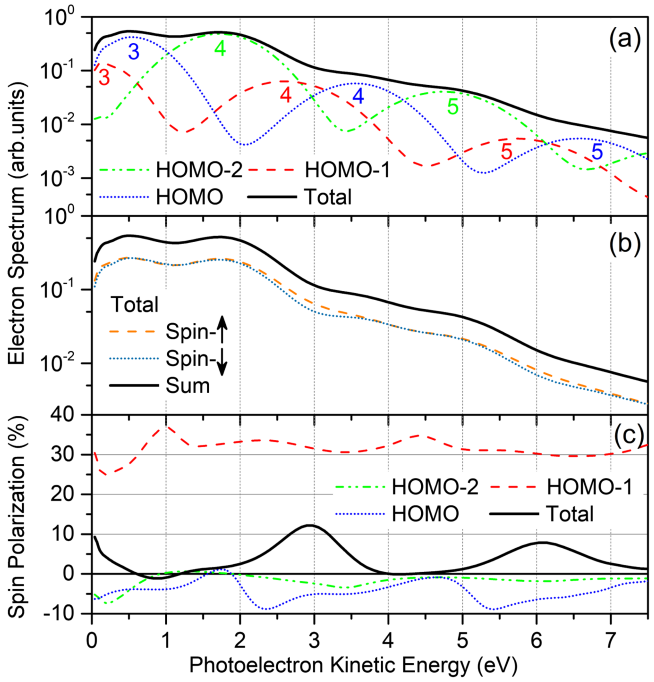


FIG. 2. Results of our calculations for randomly oriented R(−)-IMB enantiomer ionized by 395 nm circularly polarized laser pulses of $10^{13}$ W/cm$^2$ peak intensity and positive helicity. Panel (a): the total spectrum for all photoelectrons and its break down into the contributions from different molecular orbitals. The number of photons absorbed to produce each peak in the spectra is indicated by colored numbers. Panel (b): the break down of the total photoelectron spectrum into the contributions from spin-↑ and spin-↓ photoelectrons. Panel (c): individual spin polarization for each molecular orbital and the total result.

The results of the calculations for a randomly oriented $R(-)$-IMB enantiomer are collected in Fig. 2. Its panel (a) illustrates individual contribution from HOMO, HOMO-1, and HOMO-2 to the total spectrum. The five-photon ATI signal provided by these three orbitals spans from about 4 to 7 eV (as indicated by numbers in the respective colors). Further on, the four-photon ATI is present between 1 and 4 eV, while the three-photon ionization peak is located below 1 eV, and it has only HOMO and HOMO-1 contributions. Figure 2(b) shows the individual contributions to the total spectrum from the spin-↑ and spin-↓ photoelectrons. One can clearly identify three energy intervals where slightly more spin-↑ than spin-↓ photoelectrons are found. This is straightforwardly reflected in the total spin polarization, depicted in the Fig. 2(c) by the black solid curve. There, three intervals (below 1 eV, 2–4 eV, and 5–7 eV) with the positive spin polarization of up to about +12% are clearly seen. Given the complexity of the problem, it is remarkable that the computed spin polarization is in qualitative agreement with the experimental data. Noticeable disparities can, in turn, be attributed to two important limitations of the theory: the one-particle approximation for the photoelectron and the

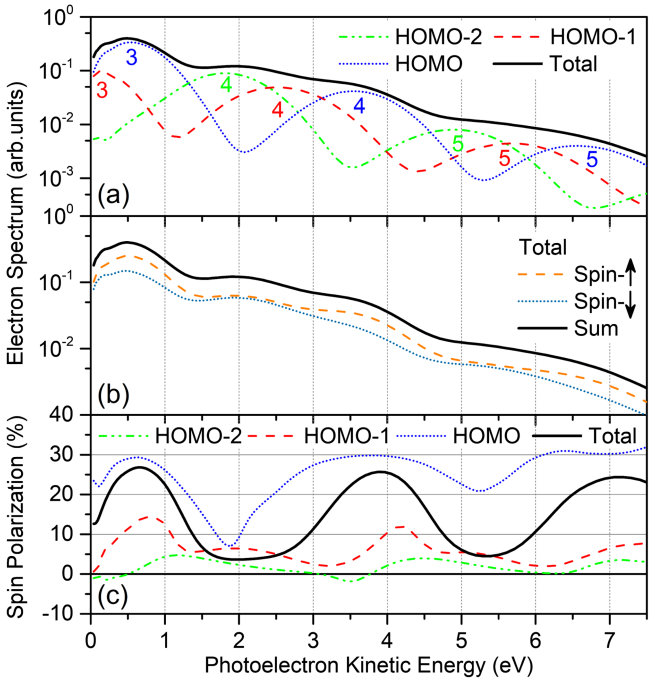


FIG. 3. The same as in Fig. 2(a)–2(c) but for the uniaxially oriented $R(-)$-IMB molecules, such that the $I$-$C$ bond is aligned along the light propagation direction.

neglect of nuclear motion. As one can see, the resulting positive spin polarization arises from the HOMO-1 contribution, as only this orbital has a positive individual spin polarization [red dashed curve in Fig. 2(c)], and HOMO and HOMO-2 have much smaller negative effect (blue dotted and green dash-dot-dotted curves). The computed contribution of HOMO-2 in the total spectrum is partly resonantly enhanced [cf., strengths of its four-photon peak and the three-photon peak of HOMO in Fig. 2(a)]. This does, however, not significantly change the final result, since its individual spin polarization almost vanishes in the respective energy regions.

Figure 3 demonstrates that the spin polarization is significantly enhanced for particular spatial orientations of the molecule. In particular, it depicts the full set of theoretical results obtained for uniaxially oriented $R(-)$-IMB enantiomer. In those calculations, the axis pointing along the bond from iodine to carbon (molecular quantization $z$ axis) was kept fixed along the light propagation direction (laboratory $z$ axis). As one can see, not only the strengths of the individual contributions from different orbitals to the spectrum [Fig. 3(a)], but also the sign of the individual spin polarizations [Fig. 3(c)] change dramatically. Here, HOMO provides an overall dominant contribution to the spectrum, and its individual spin polarization changes from small negative [for random orientations in Fig. 2(c)] to large positive values, while that from HOMO-1 stays positive but becomes much smaller. As a consequence, the spectrum of spin-↑ dominates that for spin-↓ electrons significantly [Fig. 3(b)], yielding a spin polarization of up to +27%. This parallel orientation of the molecular relative to the laboratory $z$ axes, allows us to check propensity rules for the strong-field multiphoton ionization [17,21,42–44]. In particular, the ionization probability has been suggested to be much larger if photoelectron density and polarization vector of the laser field rotate in opposite directions. Thus, for light with positive helicity, the probability to ionize counter-rotating states with negative magnetic quantum numbers $m_\ell < 0$ are predicted to dominate over that for corotating states with $m_\ell > 0$. An extended analysis of the ionized molecular orbitals nos. 89–94 demonstrated a clear overall dominance of the states with $m_\ell < 0$ in their spin-↑ components, and with $m_\ell > 0$ in the spin-↓ (see Table in Appendix).

The time-dependent single center method provides access to the angle-resolved photoionization spectra and, thus, to the PECD. A detailed analysis of the spin-↑ and spin-↓ photoelectron wave packets uncovered the following symmetry properties of the coefficients $b_L^{q,s_z}(E)$ for the expansion of the respective photoionization probabilities over the Legendre polynomials [7,8], with $E = R$ or $S$ enantiomers being mirror images of each other in the molecular $xz$ plane (i.e., we flip molecular axis $y \to -y$). In particular, keeping the light helicity $q$ and exchanging the enantiomers $R \leftrightarrow S$ yields $b_{\text{even}}^{q,s_z}(R) = b_{\text{even}}^{q,s_z}(S)$ and $b_{\text{odd}}^{q,s_z}(R) = -b_{\text{odd}}^{q,s_z}(S)$. The first rule suggests that the spin polarization does not change upon exchanging the enantiomers. This is related to the fact, that only the spherically symmetric part of SO interaction, as provided by the central iodine atom, was accounted for in the calculations (see above). We expect that this might change for a "chiral" SO interaction, like in axially chiral molecules with a helical arrangement of the SO interaction sources. The second rule, as expected, suggests that the forward-backward asymmetries in the spectra of both, spin-↑ and spin-↓ photoelectrons are opposite for two enantiomers.

In the case of keeping the IMB enantiomer fixed and flipping the light helicity $+1 \leftrightarrow -1$, we observe that $b_{\text{even}}^{+,\uparrow}(E) = b_{\text{even}}^{-,\downarrow}(E)$ and $b_{\text{odd}}^{+,\uparrow}(E) = -b_{\text{odd}}^{-,\downarrow}(E)$. The first rule suggests opposite spin polarizations for the two light helicities, as expected, and, according to the second rule, the forward-backward asymmetries change their sign simultaneously with the light helicity and spin state. Because of the latter rule, it is not straightforward to use the standard definition of the PECD [1–3]. Here, one can either compare two photoionization probabilities of the same spin polarization state and light helicity, but using two different enantiomers $I^{q,s_z}(R) - I^{q,s_z}(S)$, or one keeps the enantiomer and interchanges both, the polarization state and light helicity $I^{+,\uparrow}(E) - I^{-,\downarrow}(E)$ (both definitions are equivalent). Figure 4 depicts the computed PECD for spin-↑ and spin-↓ photoelectrons in the energy region below 2 eV (see caption of the figure for details on the data representation). Each signal is normalized to the maximal

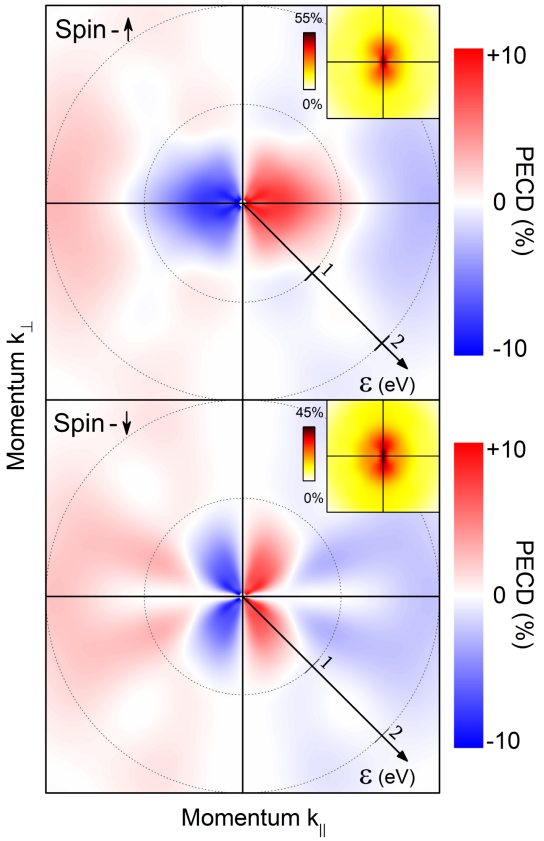


FIG. 4. Calculated multiphoton PECD of randomly oriented $R(-)$-IMB enantiomers ionized by 395 nm circularly polarized laser pulses of $10^{13}$ W/cm$^2$ peak intensity. The most intense low-energy part of the photoelectron spectrum in Fig. 2 with the photoelectron kinetic energies below 2 eV is shown. Two panels represent the chiral asymmetries separately for the spin-↑ and spin-↓ photoelectrons, each in percent relatively to the maximal pixel intensity in their own momentum distributions obtained for positive light helicity (shown in insets to each panel). Those maxima yield for spin-↑ about 55% and for spin-↓ 45% of a maximum in the total spectrum of all photoelectrons (correspond to the threshold spin polarization of about +10% in Fig. 2). The pulse propagates along $k_{||}$ from the left to the right. Note that the photoelectron momentum $k$ is set on the linear scale of the kinetic energy $\varepsilon$, as shown by the downward inclined arrows with dotted concentric circles.

intensity in the respective momentum distribution. Because of the positive spin polarization of the threshold photoelectrons, these maxima are different for the spin-↑ and spin-↓ spectra (approximately 55% and 45% of the total intensity, respectively). As one can see, both PECD have very similar magnitude of around 10%. However, the angular structures and energy dependencies of the computed multiphoton PECDs are very different, especially in its inner part below 1 eV where a sizable spin polarization is seen in Fig. 2(c).

To summarize, we observe a strong spin polarization of up to 15% for the multiphoton ionization of a chiral 1-iodo-2-methylbutane molecule with femtosecond laser pulses at a central wavelength of 395 nm. The effect is found to be enantioinsensitive. This however might change upon a "chiral" arrangement of spin-orbit-interaction sources. The observations are explained by our theory, which predicts a much stronger spin polarization for distinct molecular orientations and also very different PECDs of photoelectrons with different spin states. Because of these facts, and also taking into account that the PECD can be significantly enhanced by fixing molecular orientations (up to 20% for uniaxial orientations [45] and beyond 50% for fully fixed-in-space molecules [46]), spatially arranged chiral molecules (as, e.g., on a surface) can be used as efficient asymmetric emitters of electrons with different spin polarization.

The authors acknowledge Nityananda Sahu and Robert Berger for many valuable discussions. This work was funded by the Deutsche Forschungsgemeinschaft (DFG)—Project No. 328961117—SFB 1319 ELCH (Extreme light for sensing and driving molecular chirality).

*Appendix: Partial contributions of different $m_\ell$ states to the relevant HOMO-n of IMB molecule.—*

| Spin-↑ | HOMO-2 | HOMO-1 | HOMO | Spin-↓ |
|---|---|---|---|---|
| $m_\ell > 0$ | 29% | 11% | 23% | $m_\ell < 0$ |
| $m_\ell = 0$ | 25% | 34% | 45% | $m_\ell = 0$ |
| $m_\ell < 0$ | 46% | 55% | 32% | $m_\ell > 0$ |

*Corresponding author: doerner@atom.uni-frankfurt.de
†Corresponding author: demekhin@physik.uni-kassel.de

[1] I. Powis, Adv. Chem. Phys. **138**, 267 (2008).
[2] L. Nahon, G. A. Garcia, and I. Powis, J. Electron Spectrosc. Relat. Phenom. **204**, 322 (2015).
[3] S. Turchini, J. Phys. Condens. Matter **29**, 503001 (2017).
[4] B. Ritchie, Phys. Rev. A **13**, 1411 (1976).
[5] N. Böwering, T. Lischke, B. Schmidtke, N. Müller, T. Khalil, and U. Heinzmann, Phys. Rev. Lett. **86**, 1187 (2001).
[6] G. A. Garcia, L. Nahon, M. Lebech, J. C. Houver, D. Dowek, and I. Powis, J. Chem. Phys. **119**, 8781 (2003).
[7] C. Lux, M. Wollenhaupt, T. Bolze, Q. Liang, J. Köhler, C. Sarpe, and T. Baumert, Angew. Chem. Int. Ed. **51**, 5001 (2012).
[8] C. S. Lehmann, N. B. Ram, I. Powis, and M. H. M. Janssen, J. Chem. Phys. **139**, 234307 (2013).
[9] S. Beaulieu, A. Ferré, R. Géneaux, R. Canonge, D. Descamps, B. Fabre, N. Fedorov, F. Légaré, S. Petit, T. Ruchon, V. Blanchet, Y. Mairesse, and B. Pons, New J. Phys. **18**, 102002 (2016).
[10] M. Wollenhaupt, New J. Phys. **18**, 121001 (2016).
[11] A. Kastner, C. Lux, T. Ring, S. Züllighoven, C. Sarpe, A. Senftleben, and T. Baumert, Chem. Phys. Chem. **17**, 1119 (2016).

[12] U. Fano, Phys. Rev. **178**, 131 (1969).
[13] N. A. Cherepkov, Adv. At. Mol. Phys. **19**, 395 (1983).
[14] U. Heinzmann and J. H. Dil, J. Phys. Condens. Matter **24**, 173001 (2012).
[15] I. Barth and O. Smirnova, Phys. Rev. A **88**, 013401 (2013).
[16] A. Hartung, F. Morales, M. Kunitski, K. Henrichs, A. Laucke, M. Richter, T. Jahnke, A. Kalinin, M. Schöffler, L. Ph. H. Schmidt, M. Ivanov, O. Smirnova, and R. Dörner, Nat. Photonics **10**, 526 (2016).
[17] D. Trabert, A. Hartung, S. Eckart, F. Trinter, A. Kalinin, M. Schöffler, L.Ph. H. Schmidt, T. Jahnke, M. Kunitski, and R. Dörner, Phys. Rev. Lett. **120**, 043202 (2018).
[18] M.-M. Liu, Y. Shao, M. Han, P. Ge, Y. Deng, C. Wu, Q. Gong, and Y. Liu, Phys. Rev. Lett. **120**, 043201 (2018).
[19] K. Liu and I. Barth, Phys. Rev. A **94**, 043402 (2016).
[20] K. Liu, K. Renziehausen, and I. Barth, Phys. Rev. A **95**, 063410 (2017).
[21] Z. Nie, F. Li, F. Morales, S. Patchkovskii, O. Smirnova, W. An, N. Nambu, D. Matteo, K. A. Marsh, F. Tsung, W. B. Mori, and C. Joshi, Phys. Rev. Lett. **126**, 054801 (2021).
[22] S. Carlström, M. Bertolino, J. M. Dahlström, and S. Patchkovskii, Phys. Rev. A **106**, 042806 (2022).
[23] A. N. Artemyev, E. Kutscher, B. M. Lagutin, and Ph. V. Demekhin, J. Chem. Phys. **158**, 154115 (2023).
[24] B. Göhler, V. Hamelbeck, T. Z. Markus, M. Kettner, G. F. Hanne, Z. Vager, R. Naaman, and H. Zacharias, Science **331**, 894 (2011).
[25] K. Michaeli, N. Kantor-Uriel, R. Naaman, and D. H. Waldeck, Chem. Soc. Rev. **45**, 6478 (2016).
[26] F. Evers, A. Aharony, N. Bar-Gill, O. Entin-Wohlman, P. Hedegard, O. Hod, P. Jelinek, G. Kamieniarz, M. Lemeshko, K. Michaeli, V. Mujica, R. Naaman, Y. Paltiel, S. Refaely-Abramson, O. Tal, J. Thijssen, M. Thoss, J. M. van Ruitenbeek, L. Venkataraman, D. H. Waldeck, B. Yan, and L. Kronik, Adv. Mater. **34**, 2106629 (2022).
[27] D.-Y. Zhang, Y. Sang, T. K. Das, Z. Guan, N. Zhong, C.-G. Duan, W. Wang, J. Fransson, R. Naaman, and H.-B. Yang, J. Am. Chem. Soc. **145**, 26791 (2023).
[28] G. C. Burnett, T. J. Monroe, and F. B. Dunning, Rev. Sci. Instrum. **65**, 1893 (1994).
[29] J. J. McClelland, M. R. Scheinfein, and D. T. Pierce, Rev. Sci. Instrum. **60**, 683 (1989).
[30] A. N. Artemyev, A. D. Müller, D. Hochstuhl, and Ph. V. Demekhin, J. Chem. Phys. **142**, 244105 (2015).
[31] A. D. Müller, A. N. Artemyev, and Ph. V. Demekhin, J. Chem. Phys. **148**, 214307 (2018).
[32] A. D. Müller, E. Kutscher, A. N. Artemyev, and Ph. V. Demekhin, J. Chem. Phys. **152**, 044302 (2020).
[33] Ph. V. Demekhin, A. N. Artemyev, A. Kastner, and T. Baumert, Phys. Rev. Lett. **121**, 253201 (2018).
[34] A. N. Artemyev, E. Kutscher, and Ph. V. Demekhin, J. Chem. Phys. **156**, 031101 (2022).
[35] E. Kutscher, A. N. Artemyev, and Ph. V. Demekhin, Phys. Rev. A **107**, 013107 (2023).
[36] D. E. Manolopoulos and R. E. Wyatt, Chem. Phys. Lett. **152**, 23 (1988).
[37] T. N. Rescigno and C. W. McCurdy, Phys. Rev. A **62**, 032706 (2000).
[38] K. Schwarz, Phys. Rev. B **5**, 2466 (1972).
[39] E. Polizzi, Phys. Rev. B **79**, 115112 (2009).
[40] E. Polizzi and J. Kestyn, arXiv:1203.4031v3.
[41] A. N. Artemyev, A. I. Streltsov, and Ph. V. Demekhin, Phys. Rev. Lett. **122**, 183201 (2019).
[42] I. Barth and O. Smirnova, Phys. Rev. A **84**, 063415 (2011).
[43] T. Herath, L. Yan, S. K. Lee, and W. Li, Phys. Rev. Lett. **109**, 043004 (2012).
[44] S. Eckart, M. Kunitski, M. Richter, A. Hartung, J. Rist, F. Trinter, K. Fehre, N. Schlott, K. Henrichs, L. Ph. H. Schmidt, T. Jahnke, M. Schöffler, K. Liu, I. Barth, J. Kaushal, F. Morales, M. Ivanov, O. Smirnova, and R. Dörner, Nat. Phys. **14**, 701 (2018).
[45] M. Tia *et al.*, J. Phys. Chem. Lett. **8**, 2780 (2017).
[46] K. Fehre *et al.*, Phys. Rev. Lett. **127**, 103201 (2021).